Localized Transverse Bursts in Inclined Layer Convection

Karen E. Daniels,[1] Richard J. Wiener,[2] and Eberhard Bodenschatz[1]
[1]*Laboratory of Atomic and Solid State Physics, Cornell University, Ithaca, New York 14853, USA*
[2]*Department of Physics, Pacific University, Forest Grove, Oregon 97116, USA*
(Received 7 August 2002; published 9 September 2003)

We investigate a novel bursting state in inclined layer thermal convection in which convection rolls exhibit intermittent, localized, transverse bursts. With increasing temperature difference, the bursts increase in duration and number while exhibiting a characteristic wave number, magnitude, and size. We propose a mechanism which describes the duration of the observed bursting intervals and compare our results to bursting processes in other systems.

DOI: 10.1103/PhysRevLett.91.114501 PACS numbers: 47.20.Ky, 47.54.+r

Bursting phenomena, in which the amplitude of a nonlinear state rapidly increases and then decays, are common to nonequilibrium systems as diverse as neuronal firing [1], lasers [2], and solar cycles [3]. In the case of fluid systems, bursting has been observed in Taylor-Couette flow [4], binary fluid convection [5], and shear flow through pipes, in which it is essential to the understanding of the transition to turbulence. Models have been developed which rely on non-normal, linear interactions and nonlinear interactions [6]. However, the choice among the different mechanisms underlying intermittent bursting is still unresolved. Furthermore, bursting is usually addressed within a dynamical systems approach [7], which does not allow the treatment of bursts that are spatially localized.

In this Letter, we report data on spatially localized bursts in an experimental system, namely, inclined layer convection (ILC) [8], for which the experimental conditions are exceptionally well controlled. ILC lends itself well to detailed study: Bursts appear very close to the onset of convection, grow from an initial instability, and the spatiotemporal dynamics can be quantified. Our data show many interesting and unexplained properties across a range of parameters: spatial localization, transverse instability, weak persistence of the linear instability while bursting, and repeated cycles of growth and decay. These experimental observations need a theoretical description that in turn may lead to a better understanding of general mechanisms for bursting in nonequilibrium systems.

Inclined layer convection is a variant of Rayleigh-Bénard (thermal) convection [9], in which a fluid layer is heated from one side and cooled from the other. Tilting this layer by an angle θ results in a base state which is a superposition of a linear temperature gradient and a shear flow up along the hot plate and down along the cold. When heated beyond a critical temperature difference ΔT_c, the fluid convects due to the buoyancy of the hot fluid. As θ is increased, the buoyancy provided by the perpendicular component of gravity $g_\perp \equiv g\cos\theta$ becomes weaker and the shear flow provided by $g_\parallel$ becomes stronger. Above a codimension-two point at θ_c, the primary instability is due to this shear flow instead of buoyancy [10]. Interesting bursting behavior (see Fig. 1) has been observed in the vicinity of this codimension-two point [8].

We perform experiments in high pressure CO_2 in an apparatus similar to that described in [12], modified to allow for inclination. The gas was at a pressure of (48.26 ± 0.01) bar regulated to ± 0.005 bar with a mean temperature of $(25.00 \pm 0.05)\,^\circ$C regulated to ± 0.3 mK. Our three convection cells were of height $d = 778 \pm 2\,\mu$m and length $97.3d$. The widths in the $\hat{\mathbf{x}}$ direction are $L_1 = 10.4d$ for cell 1, $L_2 = 20.9d$ for cell 2, and $L_3 = 31.0d$ for cell 3. These parameters give a vertical viscous diffusion time of $\tau_v = d^2/\nu = (4.50 \pm 0.02)$ s, a Prandtl number $\sigma = 1.301 \pm 0.001$, and weakly non-Boussinesq conditions ($Q = 0.2$ to 0.8, as described in [9]). The planform of the convection pattern was observed via the shadowgraph technique [12] using a digital camera. The two control parameters are the angle θ and the nondimensionalized temperature difference $\epsilon \equiv (\Delta T)/(\Delta T_c) - 1$.

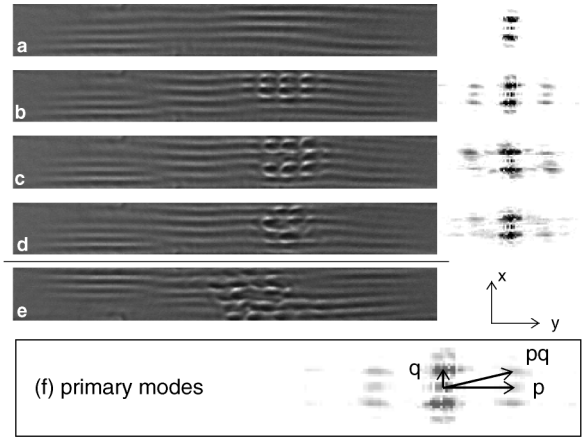

FIG. 1. (a)–(d) Sequence of background-divided shadowgraph images and associated contrast-enhanced power spectra for cell 1 at $\theta = 78°$ and $\epsilon = 0.08$: (a) quiescent, (b) modulations during early bursting, (c) developed bursting, and (d) end of burstlet. Times correspond to points marked in Fig. 3. Uphill direction is at left. (e) Disordered bursting at $\theta = 78°$ and $\epsilon = 0.09$. Also see movies in [11]. (f) Magnified power spectrum showing three primary modes.

 0031-9007/03/91(11)/114501(4)$20.00

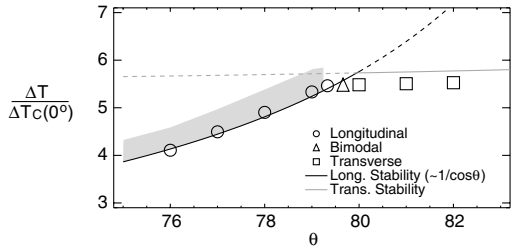

FIG. 2. Phase diagram near the codimension-two point. Stability curves are from [13]; solid lines are primary instabilities and dashed lines are extensions. Shaded area corresponds to region of data collection.

Images were collected at 27 frames/τ_v with runs of duration at least $1000\tau_v$ at various values of ϵ, θ (see Fig. 2).

The localized transverse bursts appear just below the codimension-two point at $\theta = 79.9°$ [8]. These bursts are triggered within a secondary instability in which there is already local growth of regions of high-amplitude longitudinal convection, as seen in the sequence of images in Fig. 1; a movie of the corresponding images are available online [11]. Within these regions, transverse modulations repeatedly grow and decay, becoming highly disordered in the process; this is accompanied by a noticeable shearing of the roll spectra [see Fig. 1(c)]. Eventually, this cycle of bursting ends and the system returns to quiescent, weak longitudinal rolls. The phenomenon becomes more pronounced at large ϵ, so that eventually the whole cell is bursting. Each localized patch does not spread and no global bursting was observed. At lower inclination (further from the codimension-two point) the bursting has a less-uniform wave number and is less localized (see Figs. 4 and 5), such that no sharp boundary is observed between this flow regime and that of the crawling rolls described in [8].

We describe the bursts based on the modes they excite in Fourier space, using the power spectra of background-divided images as a function of time. Sample spectra and their corresponding shadowgraph images are shown in Fig. 1, with three prominent modes: a pure $\hat{\mathbf{x}}$ mode q (strongest), a pure $\hat{\mathbf{y}}$ mode p, and a mixed mode pq which are in resonance with each other. The longitudinal rolls are composed of the pure q mode, while the transverse modulations are constructed from the p and pq modes. Higher-order modes serve to create the characteristic shape of the bursts and will be ignored here. It should be noted that the shadowgraph technique gives only a two-dimensional image of the density field, integrating through the fluid layer.

We define S_q, S_{pq}, and S_p as the power in each of these three peaks, taken as the total intensity in a fixed region of Fourier space. Figure 3(a) shows time traces of the power in each of the three modes. Prior to the beginning of each burst S_q increases in relative amplitude, as shown in Fig. 3(b). The beginning of a burst is characterized by the rapid growth of the transverse modulations (via S_{pq}). Since a resonance condition is observed between the three modes and the S_p mode grows after a delay of about $0.5\tau_v$, it is possible that a nonlinearity between S_q and S_{pq} is responsible for the growth in S_p.

The measured wave number p of the transverse modulations is shown in Fig. 4 and observed to be approximately constant. Intriguingly, the observed wave number falls just below the value $p = p_c/2$ (shown as a dashed line) obtained from stable transverse rolls with wave number p_c at $\theta = 80°$. While the appearance of this bursting phenomena close to the stability curve for transverse rolls suggests that a related shear instability is playing a role, experimental observations do not show a mode subharmonic to p_c in the bursting spectra (see Fig. 1).

Using Fourier decomposition, we determined the area of each cell occupied by transverse bursting and found the width of the region for those instances in which only a single burst was present. As shown in Fig. 5, the bursts generally have a characteristic width of $15d$ in the transverse direction and length $20d$ in the longitudinal. Bursts are smaller in cell 1 [see Fig. 5(a)], where they fill the cell in the $\hat{\mathbf{x}}$ (transverse) direction. They are larger both away from the codimension-two point [Fig. 5(b)] and for increased ϵ [Fig. 5(c)], as shown exemplarily for cell 2. Hereafter, the investigation of bursting dynamics has been restricted to cell 1 since this cell is sufficiently narrow to contain only single localized bursts, allowing automated analysis. The behavior in cells 2 and 3 was observed to be similar except for the presence of multiple simultaneous bursts. For cells 1, 2, and 3 at $\theta = 78°$, the onset of bursting was observed to occur at $\epsilon = 0.075$, $\epsilon = 0.02$, and $\epsilon = 0.04$, respectively.

The time series in Fig. 3(a) shows two important temporal features: (i) intermittent, alternating periods of

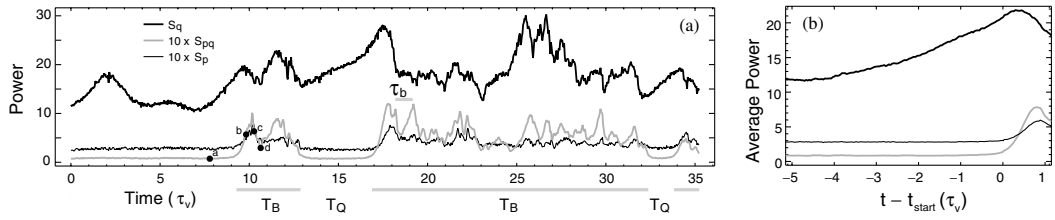

FIG. 3. (a) Sample segment of $S_q(t)$, $S_{pq}(t)$, and $S_p(t)$ at $\epsilon = 0.08$ and $\theta = 78°$ in cell 1. Gray bars indicated bursting; time intervals T_B, T_Q, and τ_b defined in text. Labeled black dots correspond to the images in Fig. 1. (b) Ensemble average $\langle S(t - t_{\text{start}})\rangle$ over all bursts where t_{start} is the rising edge of S_{pq} for each burst. Power is in same arbitrary units for both figures.

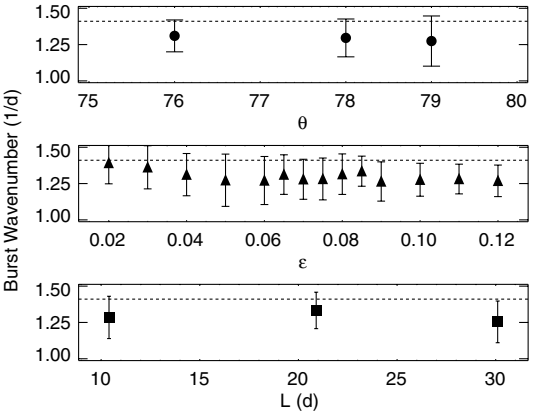

FIG. 4. Wave number of transverse bursts p (determined from power spectra) as a function of θ, ϵ, and cell length L. In each graph the wave number is plotted against the given variable, and averaged over the other two. Dashed lines are $p_c/2$ for $p_c = (2.82 \pm 0.04)d$ at $\epsilon = 0$ (onset) and $\theta = 80°$ (weak dependence on θ).

quiescence and bursting and (ii) burstlets characterized by peaks and troughs within the bursting intervals. As $S_{pq}(t)$ rises at the beginning of a burstlet, the pattern exhibits the increasingly well-defined modulations shown in Fig. 1(b). When S_{pq} peaks, these modulations become spatially disordered on short time scales, moving rapidly within the underlying rolls. While the general roll pattern is retained in any single image [see Figs. 1(c) and 1(d)], the roll segments themselves move within the localized bursting region [11]. At higher ϵ and θ, both of which increase the shear flow, this disorder is increased [see Fig. 1(e)]. From the disordered state, the modulations either decay—resulting in the end of the bursting interval—or grow again, creating another burstlet within the same interval. A succession of such events is suggestive of the presence of a limit cycle. Stochastic limit cycles have been previously described in [7,14], relying on a random forcing effect such as pressure fluctuations to produce random events with a single, well-defined mean rate.

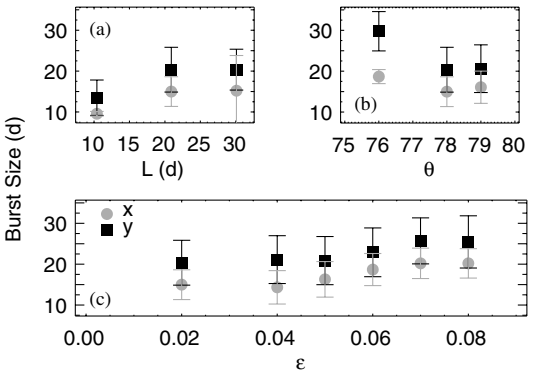

FIG. 5. Burst width ($\hat{\mathbf{x}}$, gray) and length ($\hat{\mathbf{y}}$, black) directions: (a) vs cell width L at onset of bursting for $\theta = 78°$, (b) vs θ at onset of bursting in cell 2, and (c) vs ϵ in cell 2 at $\theta = 78°$.

To determine the quiescent and bursting intervals, we set a threshold for $S_{pq}(t)$ above which the system was considered to be bursting. Because the onset and decay of the burst was sharp, the results were not sensitive to the choice of threshold over a reasonable range of values. Using this information, we examined the duration of quiescent intervals T_Q, bursting intervals T_B. Burstlets are separated by intervals τ_b within the T_B, with burstlet peaks identified by local maximum. Examples of the determined bursting intervals are shown by the gray bars at the bottom of Fig. 3(a). Sample probability distribution functions (PDFs) and mean values as a function of ϵ are plotted in Fig. 6. The quiescent intervals T_Q were longest close to the onset of bursting, and decreased until they were no longer detectable at higher ϵ. Conversely, the bursting intervals T_B grow with ϵ. The combined effect is that at high ϵ the whole cell is in a perpetual state of bursting since each localized burst lives longer and new ones begin sooner. All of these trends hold at other values of ϵ and θ as well.

It is interesting to compare the bursting in ILC with that of Taylor-Couette flow, where similar behavior has been observed [4]. In both systems, bursts appear to be caused by a secondary instability whose growth above a threshold triggers transient disorder. In Taylor-Couette flow, once the turbulence has begun it destroys (sometimes globally) the underlying rolls which were feeding it, and thus it dies away after a well-defined period of

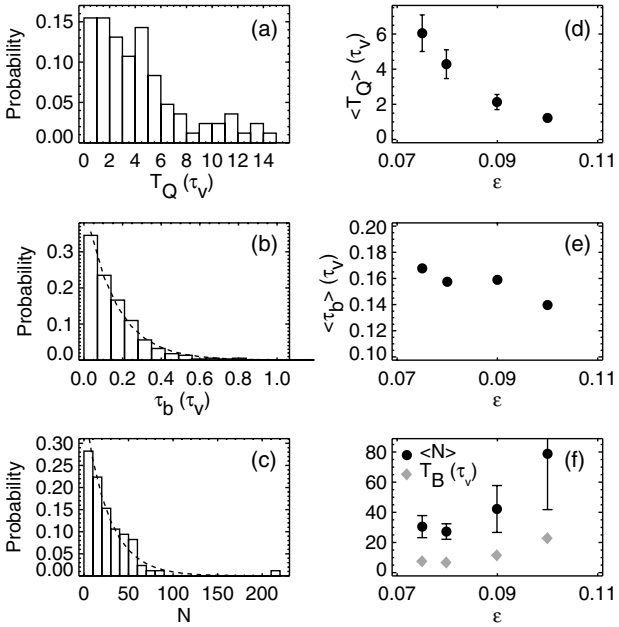

FIG. 6. (a),(b),(c) Sample PDFs of T_Q, τ_b, and N, respectively, at $\epsilon = 0.08$ and $\theta = 78°$. (b) Dashed line is exponential distribution fit to data excluding the first bin. (c) Dashed line is Eq. (3) plotted from the measured mean. (d) Mean quiescent period as a function of ϵ at $\theta = 78°$. (e) Effective (from fit) mean burstlet period and (f) mean number of burstlets and mean bursting interval as a function of ϵ at $\theta = 78°$.

time. Contrarily, the bursts in ILC cause only local disorder and fail to globally trigger turbulence. Because the modulation and rolls appear to be incompletely destroyed [see Fig. 3(a)], they are able to grow back up again after they decay; this may explain the presence of repeated burstlets. As a result, the bursting interval T_B is not constant as was observed for the Taylor-Couette bursts but instead increases with ϵ, as shown in Fig. 6(f). A second similarity between the two systems is the trend towards longer quiescent periods T_Q at lower ϵ [see Fig. 6(d)]. Quantitatively, Taylor-Couette bursts exhibit $\langle T_Q \rangle \sim 1/\epsilon$ behavior based on a constant growth rate of the secondary instability [4], but the nonconstant T_B may destroy such a relationship here.

To create cycles of burstlets within each bursting interval, a second mechanism is needed, possibly sensitive to noise. At each ϵ and θ, the PDF of τ_b [see Fig. 6(b)] exhibits a negative exponential distribution,

$$\mathcal{P}(\tau_b) = \frac{e^{-\tau_b/\langle \tau_b \rangle}}{\langle \tau_b \rangle}, \tag{1}$$

where $\langle \tau_b \rangle$ is the mean waiting period of a Poisson process generating the bursts. Because the lowest τ_b bin is underreported due to the finite sampling of the time series, $\langle \tau_b \rangle_{\text{eff}}$ is found instead by fitting the negative exponential to all data except for the first bin.

This description can also explain why T_B is not constant. In a Poisson process, the events are memoryless: The wait time for the next event is independent of how long the system has already been waiting. If a new burstlet were not generated before the decay to quiescence, the modulations would die away and the burst interval would be over. Assuming a constant, unknown decay time τ_d, the probability distribution for N burstlets for which each τ_b is no more than τ_d is calculated using the cumulative distribution of Eq. (1), $\mathcal{P}(\tau_b \leq \tau_d) = 1 - e^{-\tau_b/\tau_d}$.

$$\mathcal{P}(N) = \frac{(1 - e^{-\tau_d/\langle \tau_b \rangle})^N}{e^{\tau_d/\langle \tau_b \rangle} - 1}. \tag{2}$$

This distribution contains a single parameter $\langle N \rangle \equiv e^{\tau_d/\langle \tau_b \rangle}$, which can be measured directly from the experimental $\mathcal{P}(N)$. Equation (2) then reduces to

$$\mathcal{P}(N) = \frac{(\langle N \rangle - 1)^{N-1}}{\langle N \rangle^N}, \tag{3}$$

where $\langle N \rangle$ is the measured mean number of burstlets per interval. This formulation allows for comparison with the observed data with no fit parameters. Figure 6(c) shows good agreement with this model, as do plots at other parameter values. Therefore, our results are consistent with the burstlets being Poisson-distributed events.

Transverse bursts in inclined layer convection show many interesting and unexplained properties across a range of parameters: spatial localization, transverse instability, weak persistence of the linear instability while bursting, and repeated cycles of growth and decay once triggered. Initial theoretical investigations [13] show that a three-mode resonance cannot describe the bursting, and it remains to be seen whether non-normal properties of the system are important. This system is ideally suited for theoretical progress as the instabilities occur very close to the onset of convection and can also be characterized through numerical simulations [15]. We hope that these experiments will motivate theoretical studies which both explain this very interesting phenomenon and lead to a better understanding of the general properties of localized bursting in nonequilibrium systems.

We wish to thank W. Pesch and J. Brink for sharing results from stability analysis and full numerical simulations and J. P. Sethna for fruitful discussions. We are grateful to NSF for support under DMR-0072077 and the IGERT program in nonlinear systems, DGE-9870631.

[1] T. R. Chay, Y. S. Fan, and Y. S. Lee, Int. J. Bifurcation Chaos **5**, 595 (1995).
[2] R. Meucci, A. D. Garbo, E. Allaria, and F. T. Arecchi, Phys. Rev. Lett. **88**, 144101 (2002).
[3] P. Charbonneau, Sol. Phys. **199**, 385 (2001).
[4] K. Coughlin, C. F. Hamill, P. S. Marcus, and H. L. Swinney (unpublished); K. Coughlin and P. S. Marcus, Phys. Rev. Lett. **77**, 2214 (1996).
[5] J. Moehlis and E. Knobloch, Phys. Rev. Lett. **80**, 5329 (1998); T. S. Sullivan and G. Ahlers, Phys. Rev. A **38**, 3143 (1988).
[6] S. Grossmann, Rev. Mod. Phys. **72**, 603 (2000); F. Waleffe, Phys. Fluids **7**, 3060 (1995).
[7] E. Knobloch and J. Moehlis, in *Nonlinear Instability, Chaos and Turbulence, Vol. II*, edited by L. Debnath and D. Riahi (Computational Mechanics Publications, Southampton, 2000), pp. 237–87.
[8] K. E. Daniels, B. B. Plapp, and E. Bodenschatz, Phys. Rev. Lett. **84**, 5320 (2000).
[9] E. Bodenschatz, W. Pesch, and G. Ahlers, Annu. Rev. Fluid Mech. **32**, 709 (2000).
[10] R. M. Clever and F. H. Busse, J. Fluid Mech. **81**, 107 (1977); K. Fujimura and R. E. Kelly, J. Fluid Mech. **246**, 545 (1993); J. E. Hart, J. Fluid Mech. **47**, 547 (1971).
[11] See EPAPS Document No. E-PRLTAO-91-016331 for movies of bursting state at $\theta = 30°$, $\epsilon = 0.08$, $\Delta T = 2.462$. A direct link to this document may be found in the online article's HTML reference section. The document may also be reached via the EPAPS homepage (http://www.aip.org/pubservs/epaps.html) or from ftp.aip.org in the directory /epaps/. See the EPAPS homepage for more information.
[12] J. R. de Bruyn *et al.*, Rev. Sci. Instrum. **67**, 2043 (1996).
[13] W. Pesch (private communication).
[14] F. H. Busse, in *Turbulence and Chaotic Phenomena in Fluids*, edited by T. Tatsumi (Elsevier, Amsterdam, 1984).
[15] O. Brausch, Ph.D. thesis, Universität Bayreuth, 2001.